

Spin-phonon interaction and short range order in $\text{Mn}_3\text{Si}_2\text{Te}_6$

S. Djurdjić Mijin,¹ A. Šolajić,¹ J. Pešić,¹ Y. Liu,^{2,*} C. Petrovic,²
M. Bockstedte,³ A. Bonanni,⁴ Z. V. Popović,^{1,5} and N. Lazarević¹

¹*Institute of Physics Belgrade, University of Belgrade, Pregrevica 118, 11080 Belgrade, Serbia*

²*Condensed Matter Physics and Materials Science Department,
Brookhaven National Laboratory, Upton, NY 11973-5000, USA*

³*Institute for Theoretical Physics, Johannes Kepler University Linz, Altenbergerstr. 69, 4040 Linz, Austria*

⁴*Institute of Semiconductor and Solid-State Physics,*

Johannes Kepler University Linz, Altenbergerstr. 69, 4040 Linz, Austria

⁵*Serbian Academy of Sciences and Arts, Knez Mihailova 35, 11000 Belgrade, Serbia*

(Dated: September 7, 2022)

The vibrational properties of ferrimagnetic $\text{Mn}_3\text{Si}_2\text{Te}_6$ single crystals are investigated using Raman spectroscopy and density functional theory calculations. Eighteen Raman-active modes are identified, fourteen of which are assigned according to with the trigonal symmetry. Four additional peaks, obeying the A_{1g} selection rules, are attributed to the overtones. The unconventional temperature evolution of the A_{1g}^5 mode self-energy suggests a competition between different short-range magnetic correlations that significantly impact the spin-phonon interaction in $\text{Mn}_3\text{Si}_2\text{Te}_6$. The research provides a comprehensive insight to the lattice properties, studies their temperature dependence and shows the arguments for existence of competing short-range magnetic phases in $\text{Mn}_3\text{Si}_2\text{Te}_6$.

I. INTRODUCTION

Layered magnetic van der Waals materials have lately received widespread attention due to their potential application in spintronics, magneto-electronics, data storage and biomedicine [1–7]. Recent experimental confirmation of a long-range magnetism persisting down to a monolayer in CrI_3 [8] further affirmed a these materials as platform for magneto-optoelectronic devices [9], and as candidates for studying low-dimensional magnetism [10].

$\text{Mn}_3\text{Si}_2\text{Te}_6$ single crystals were first synthesized in 1985 [11]. However, few studies were carried out on this compound since. It was only recently that the attention has shifted to them, mainly through comparisons with quasi-two-dimensional materials, specifically CrSiTe_3 . The vast majority of recent studies were focused on explaining the magnetism in $\text{Mn}_3\text{Si}_2\text{Te}_6$ and determining its crystal structure. It was revealed that $\text{Mn}_3\text{Si}_2\text{Te}_6$ crystalizes in a trigonal structure described by the $P\bar{3}1c$ (No. 163) space group [11, 12]. According to various magnetization studies, $\text{Mn}_3\text{Si}_2\text{Te}_6$ is an insulating ferrimagnetic with Currie temperature T_c between 74 K –78 K [12–15]. First principle calculations suggested a competition between ferrimagnetic ground state and three additional magnetic configurations, originating from antiferromagnetic exchange for the three nearest Mn-Mn pairs [15]. Additionally, both magnetization and diffuse neutron scattering experiments point at the existence of strong spin correlations well above T_c , which may be associated with short-range order or to the preserved correlated excitations in the paramagnetic region [12, 15].

Here we present an experimental and theoretical Raman scattering study of $\text{Mn}_3\text{Si}_2\text{Te}_6$ single crystals, with the focus on phonon properties in the temperature range from 80 K to 320 K. Out of eighteen observed modes, fourteen ($5A_{1g} + 9E_g$) are identified and assigned in agreement with the $P\bar{3}1c$ space group. Phonon energies are in a good agreement with the theoretical predictions. Two most prominent Raman modes, A_{1g}^4 and A_{1g}^5 , are used to study the temperature evolution of phonon properties, and reveal three subsequent phase transitions at $T_1 = 142.5$ K, $T_2 = 190$ K and $T_3 = 285$ K. Furthermore, the A_{1g}^5 mode exhibits strong asymmetry, originating from enhanced spin-phonon coupling. Interestingly, the A_{1g}^5 phonon line is symmetric in the temperature range T_1 – T_2 , while becoming more asymmetric above T_3 , indicating that the strength of spin-phonon interaction changes with temperature. We speculate, that the observed phenomenon, shown in A_{1g}^5 phonon, originates from the shift in dominance between competing magnetic states, that are found to be very close in energy [15].

II. EXPERIMENTAL AND COMPUTATIONAL DETAILS

The $\text{Mn}_3\text{Si}_2\text{Te}_6$ single crystal samples used in this study are prepared according to the procedure described in Ref. [12]. The Raman spectra have been obtained with a Tri Vista 557 spectrometer with a 1800/1800/2400 groves/mm diffraction grating combination in a backscattering configuration. The 514 nm line of a Coherent Ar^+/Kr^+ ion laser is utilized as excitation source. The direction of the incident (scattered) light coincides with the crystallographic c axis. Laser-beam focusing is achieved through a microscope objective with $50\times$ magnification. The temperature-dependent Raman scatter-

* Present address: Los Alamos National Laboratory, Los Alamos, New Mexico 87545, USA

ing measurements have been performed under high vacuum (10^{-6} mbar), with the sample being placed inside of a KONTI CryoVac continuous Helium flow cryostat with a 0.5 mm thick window. The samples are cleaved in air before being placed into the cryostat. The obtained Raman spectra are corrected by a Bose factor. The spectrometer resolution is comparable to a Gaussian width of 1 cm^{-1} .

The calculations are based on the density functional theory (DFT) formalism as implemented in Vienna Ab initio Simulation Package (VASP) [16–19], with the plane wave basis truncated at a kinetic energy of 520 eV, using Perdew-Burke-Ernzerhof (PBE) exchange-correlation functional [20] and Projector augmented wave (PAW) pseudopotentials [21, 22]. The Monkhorst and Pack scheme of k point sampling is employed to integrate over the first Brillouin zone with $12 \times 12 \times 10$ at the Γ -centered grid. The convergence criteria for energy and force have been set to 10^{-6} eV and $0.001 \text{ eV}\text{\AA}^{-1}$, respectively. The DFT-D2 method of Grimme is employed for van der Waals (vdW) corrections [23]. The vibrational modes are calculated using density functional perturbation theory implemented in VASP and Phonopy [24]. Previous DFT results found the energy of the ferrimagnetic state to be well above an eV per Mn below that of the non-magnetic state [15] thus this configuration is considered in this study.

III. RESULTS AND DISCUSSION

A. Polarization dependence

$\text{Mn}_3\text{Si}_2\text{Te}_6$ crystalizes in a trigonal $P\bar{3}1c$ crystal structure [11, 12]. The Wyckoff positions of the atoms and their contributions to the Γ -point phonons, together with the corresponding Raman tensors, are listed in Table II. In total, there are sixteen Raman-active modes ($5A_{1g} + 11E_g$) and seventeen infrared-active modes ($6A_{2u} + 11E_u$). According to the Raman tensors presented in Table II, E_g symmetry modes can be observed in the Raman spectra measured in both parallel and crossed polarization configurations, whereas A_{1g} modes arise only for those in parallel polarization configuration.

As depicted in Fig. 1, nine phonon lines are observed in parallel polarization configuration only, and identified as A_{1g} symmetry modes. According to the symmetry analysis only five A_{1g} symmetry modes are expected, resulting in four excess modes at 53.3 cm^{-1} , 57.9 cm^{-1} , 95.3 cm^{-1} and 366.7 cm^{-1} . These modes may arise from infra-red/silent phonons activated by disorder and from the relaxation of the symmetry selection rules [25–28]. However, it is more likely they are overtones. Overtones are always observable in A symmetries, and can become observable in Raman spectra due to disorder and/or enhanced coupling of the phonons to other excitations like in the case of spin-phonon coupling [29].

Aside from the discussed A_{1g} symmetry modes, our

TABLE I. Wyckoff positions of atoms and their contributions to the Γ -point phonons together with the corresponding Raman tensors for the $P\bar{3}1c$ space group of $\text{Mn}_3\text{Si}_2\text{Te}_6$.

Space group: $P\bar{3}1c$	
Atoms	Irreducible representations
Mn ($2c$)	$A_{2g} + A_{2u} + E_g + E_u$
Mn ($4f$)	$A_{1g} + A_{1u} + A_{2g} + A_{2u} + 2E_g + 2E_u$
Si ($4e$)	$A_{1g} + A_{1u} + A_{2g} + A_{2u} + 2E_g + 2E_u$
Te ($12i$)	$3A_{1g} + 3A_{1u} + 3A_{2g} + 3A_{2u}$ $+ 6E_g + 6E_u$
Raman tensors	
	$A_{1g} = \begin{pmatrix} a & & \\ & a & \\ & & b \end{pmatrix}$
	${}^1E_g = \begin{pmatrix} c & & \\ & -c & d \\ & d & \end{pmatrix}$ ${}^2E_g = \begin{pmatrix} & -c & -d \\ -c & & \\ d & & \end{pmatrix}$

spectra host nine modes which obey the E_g selection rules. Therefore, nine out of the expected eleven E_g modes have been singled out and identified. The absence of two E_g modes might be attributed to their low intensity and/or the finite resolution of the spectrometer.

Calculated and experimental phonon energies are collected in Table II, and are found to be in good agreement with each other, with discrepancy being below 8% for all observed modes.

Our data significantly differ from those presented in Ref. [14] where two Raman active modes were reported, one at 118.4 cm^{-1} and the other at 136.9 cm^{-1} , assigned as E_g and A_{1g} , respectively. The E_g and A_{1g} modes in our spectra closest (in terms of energy) to those reported in Ref. [14] are the peaks at ~ 114.3 and 135.4 cm^{-1} (Table II). Although the discrepancy in phonon energy is not significant, the observed phonon linewidths strongly deviate from those presented in Ref. [14]. A possible explanation for the discrepancy is the presence of TeO_2 in samples presented in Ref. [14], as the peaks reported there match rather well with the Raman response of TeO_2 (Fig. 1). In order to avoid potential contamination in our study, measurements have been repeated on multiple crystals, and no oxide traces have been identified in the spectra.

B. Temperature dependence

Some of the modes represented in Fig. 1 exhibit an asymmetric lineshape. Although, the appearance of a mode asymmetry can be attributed to the presence of defects [30] this would have a significant impact also on the line widths of other modes in spectrum, which is not the case here. The asymmetry may arise from phonon-

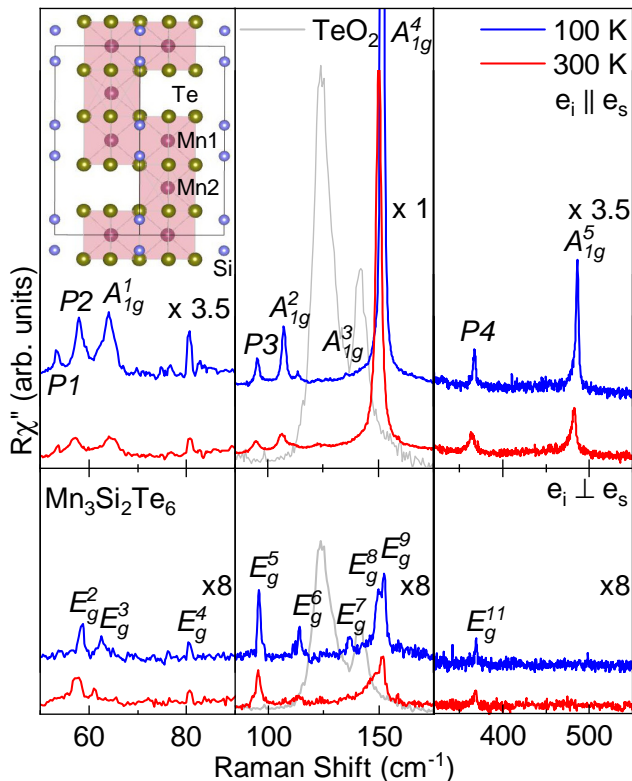


FIG. 1. Raman spectra of $\text{Mn}_3\text{Si}_2\text{Te}_6$ single crystal measured in two scattering geometries at $T=100$ K (blue solid line) and $T=300$ K (red solid lines). Peaks observed in both geometries are identified as E_g modes, whereas peaks observed only for the parallel polarization configuration are assigned as A_{1g} modes. Grey line: TeO_2 spectrum at 300 K, scaled for clarity.

continuum coupling, *e.g.* spin-phonon. The lineshape originating from such a coupling is given by the Fano profile [31]:

$$I(\omega) = I_0 \frac{(q+\epsilon)^2}{1+\epsilon^2},$$

where $\epsilon(\omega)=2(\omega-\omega_0)/\Gamma$. Here, ω_0 is the phonon frequency in the absence of interaction, Γ is the full width at the half maximum (FWHM), I_0 is the amplitude and q is the Fano parameter. The Fano parameter and FWHM depend on the interaction strength between the phonon and the continuum, and therefore can be used as its indicator. To include the finite spectral resolution of the experimental setup, the Fano profile is convoluted with a Gaussian function as demonstrated in Ref. [29].

The high intensity peak at 486.7 cm^{-1} , identified as the A_{1g}^5 symmetry mode, does not overlap with any other mode. The quantitative analysis of this peak is performed using both the symmetric Voigt profile and the Fano-Gaussian convolution mentioned above. The comparison between two models and the experimental data at 80 K and 300 K are presented in Fig. 2 (a) and (b), respectively. The asymmetric lineshapes provide a sat-

TABLE II. Phonon symmetries and phonon frequencies of $\text{Mn}_3\text{Si}_2\text{Te}_6$ phonons. The experimental values are determined at 100 K. All calculations have been performed at zero 0 K. The experimental uncertainty is 0.3 cm^{-1} .

Space group $P\bar{3}1c$			
n_0	Symm.	Exp. (cm^{-1})	Calc. (cm^{-1})
1	E_g^1	-	53.1
2	$P1$	53.3	-
3	$P2$	57.9	-
4	E_g^2	58.7	58.5
5	E_g^3	62.6	61.8
6	A_{1g}^1	64.2	62.3
7	E_g^4	80.4	82.7
8	$P3$	95.3	-
9	E_g^5	95.9	90.3
10	A_{1g}^2	107.3	104.3
11	E_g^6	114.0	106.5
12	A_{1g}^3	135.4	134.2
13	E_g^7	136.6	136.1
14	E_g^8	149.8	143.4
15	A_{1g}^4	151.8	147.3
16	E_g^9	152.6	146.6
17	E_g^{10}	-	352.7
18	$P4$	366.7	-
19	E_g^{11}	368.7	354.5
20	A_{1g}^5	486.7	475.83

isfactory description of the measured phonon line shape, suggesting the presence of an additional scattering mechanism in $\text{Mn}_3\text{Si}_2\text{Te}_6$.

The spectral region of the A_{1g}^5 Raman-active mode in the temperature range of interest is presented in Fig. 3 (a). The blue solid lines represent fits to the experimental data obtained using the Fano-Gaussian line shape. Temperature dependence of the phonon energy, line width, and the Fano parameter $|q|$ of the A_{1g}^5 mode are depicted in Fig. 3 (c), (d) and (e), respectively. By increasing the temperature above 80 K, the A_{1g}^5 mode broadens and softens up to $T_1=142.5$ K, where it abruptly narrows and shifts to higher energies followed by further softening and narrowing up to $T^*=160$ K. Additional heating leads to a broadening and hardening before the drop in phonon energy at $\sim T_2=190$ K. In the region T_2 the mode softens and broadens with additional jump in phonon energy at $T_3=285$ K. A similar trend is also observed for the A_{1g}^4 mode, as evidenced in Fig. 3 (b).

This intriguing temperature dependence is also manifested in the asymmetry *i.e.* Fano parameter $|q|$ [Fig. 3 (d)] of the A_{1g}^5 peak. At the lowest experimental temperature, 80 K, the A_{1g}^5 mode exhibits strong asymmetry with a Fano parameter $|q|=9.9$. Upon heating the sample to $\sim T_1$ a Fano parameter remains nearly constant

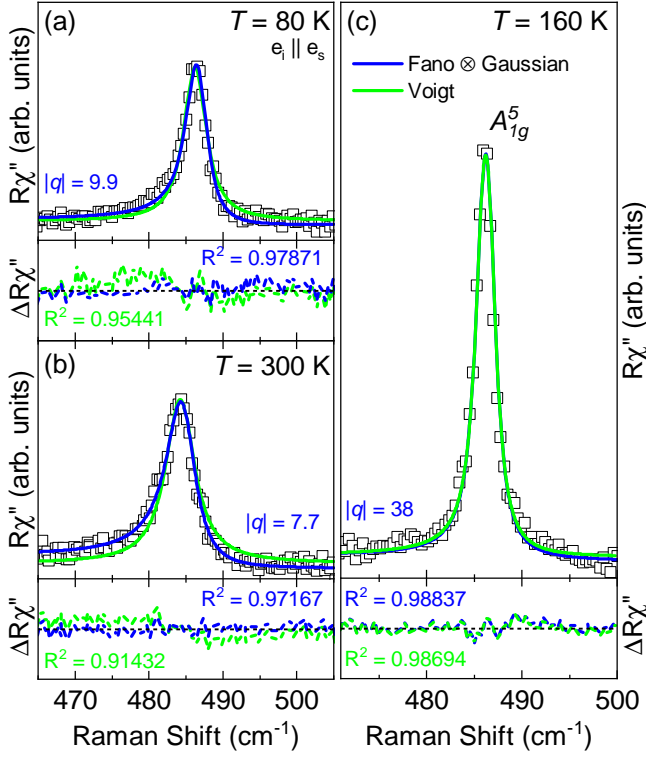


FIG. 2. Raman response as a function of the Raman shift. Quantitative analysis of the A_{1g}^5 mode at temperatures as indicated. (a) and (b) The blue solid lines represent the line shape obtained as a convolution of Fano profiles and Gaussian, whereas the green solid lines represent Voigt profiles. (c) Comparison between asymmetric (deep blue) and symmetric (light blue) line shapes obtained as a Fano-Gaussian convolution and a Voigt profile. Experimental data is represented by open squares.

before the significant increase in the temperature range between T_1 and T^* resulting in a symmetric lineshape ($|q|=38$, Fig.3 (c)). Further temperature increase leads to a strong decrease of $|q|$ up to T_2 , where the asymmetry is restored ($|q|=9.9$) remaining almost constant up to T_3 . At higher temperatures, the lineshape becomes more asymmetric, reaching $|q| \sim 8$ at the highest experimentally accessible temperature $T=320$ K.

While the ferrimagnetic order in $Mn_3Si_2Te_6$ is established only at $T_c=78$ K [12, 14], the asymmetry of the mode can be traced to enhanced spin-phonon interaction related to short-range correlation [25, 32, 33], that can survive up to temperatures well above T_c , similarly to $Mn_3Si_2Te_6$'s 2D analog $CrSiTe_3$ [34]. Based on the results presented in Ref. [15], we may speculate that these short-range correlations are likely in terms of the antiferromagnetic dimers and/or trimers between different Mn layers, Mn1 and Mn2 (as depicted in Fig. 1) in the paramagnetic background. However, this alone cannot explain sudden changes in the properties of the A_{1g}^5 phonon mode. Rather the existence of competing short-range magnetic phases may be responsible for the observed be-

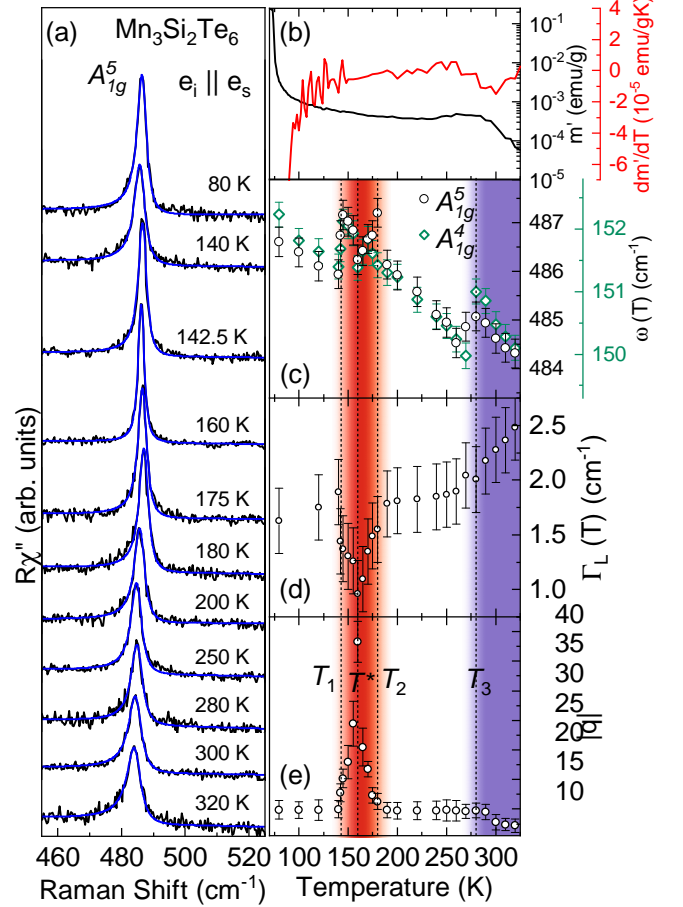


FIG. 3. (a) The spectral region of the A_{1g}^5 Raman-active mode of $Mn_3Si_2Te_6$ at indicated temperatures measured in the parallel polarization configuration. Green solid lines represent line shapes obtained as a convolution of the Fano line shape and Gaussian, calculated to fit the experimental data. (b) Temperature dependence of ac susceptibility real part $m'(T)$ and its temperature derivative plotted as a function of temperature with $\mathbf{H} \parallel \mathbf{ab}$. Temperature dependence of (c) the energy of the A_{1g}^4 and A_{1g}^5 as well as (d) the line width, and (e) the Fano parameter $|q|$ of the A_{1g}^5 mode.

havior of the phonon modes. The first phonon mode anomaly at $T_3=285$ K corresponds to the anomaly in $m'(T)_{ab}$ [Fig. 3 (b)] and can be seen as the outlet of additional short-range order in the paramagnetic domains [35] and possibly change of their nature of previously established ones. The onset in temperature with the magnetization anomaly near 330 K [14, 36] is likely the consequence of local disorder. At T_2 $Mn_3Si_2Te_6$ becomes locally magnetically frustrated resulting in the change in magnetostriction and rapid decrease of spin-phonon interaction that is manifested in the strong evolution of the phonon self-energy (Fig. 3). At this temperature both magnetoresistance and nonlinearity of Hall resistance become observable [36]. In this scenario, by further lowering the temperature, at T_1 new short range magnetic order, likely antiferromagnetic, is established

and the strong spin-phonon interaction is established. In order to fully understand the complex evolution of the short-range magnetic correlation in $\text{Mn}_3\text{Si}_2\text{Te}_6$ that is manifested through the anomalous temperature development of A_{1g}^5 mode, further investigations are required.

IV. CONCLUSION

The lattice dynamic in single crystalline $\text{Mn}_3\text{Si}_2\text{Te}_6$ using Raman spectroscopy is analyzed. Five A_{1g} modes and nine E_g modes are observed and assigned according to the $P\bar{3}1c$ symmetry group. Four additional peaks to ones assigned to $P\bar{3}1c$ symmetry group, obeying A_{1g} selection rules, are attributed to overtones. The pronounced asymmetry of the A_{1g}^5 phonon mode at 100 K and 300 K. The unconventional temperature evolution of the A_{1g}^5 Raman mode reveals three successive, possibly magnetic, phase transitions that significantly impact the strength of the spin-phonon interaction in $\text{Mn}_3\text{Si}_2\text{Te}_6$. These are likely caused by the competition between the various magnetic states, close in energy. This study provides a comprehensive insight into the lattice properties,

their temperature dependence and shows arguments for the existence of the competing short-range magnetic phases in $\text{Mn}_3\text{Si}_2\text{Te}_6$.

ACKNOWLEDGEMENTS

The authors acknowledge funding provided by the Institute of Physics Belgrade, through a grant from the Ministry of Education, Science and Technological Development of the Republic of Serbia, Project F-134 of the Serbian Academy of Sciences and Arts, the Science Fund of the Republic of Serbia, PROMIS, 6062656, Strained-FeSC, Austrian Science Fund (FWF) through the Project No. P31423, and the support of Austrian Academy of Sciences' Joint Excellence In Science And Humanities (JESH) Program (JP). DFT calculations were performed using computational resources at Johannes Kepler University (Linz, Austria). Materials synthesis was supported by the U.S. DOE-BES, Division of Materials Science and Engineering, under Contract DE-SC0012704 (BNL).

-
- [1] Z. Guguchia, Unconventional magnetism in layered transition metal dichalcogenides, *Condensed Matter* **5**, 10.3390/condmat5020042 (2020).
- [2] Q. H. Wang, K. Kalantar-Zadeh, A. Kis, J. N. Coleman, and M. S. Strano, Electronics and optoelectronics of two-dimensional transition metal dichalcogenides, *Nature Nanotechnology* **7**, 699 (2012).
- [3] W. Han, R. K. Kawakami, M. Gmitra, and J. Fabian, Graphene spintronics, *Nature Nanotechnology* **9**, 794 (2014).
- [4] W. Zhang, R. Mazzarello, M. Wuttig, and E. Ma, Designing crystallization in phase-change materials for universal memory and neuro-inspired computing, *Nature Reviews Materials* **4**, 150 (2019).
- [5] C. Zhu, G. Yang, H. Li, D. Du, and Y. Lin, Electrochemical sensors and biosensors based on nanomaterials and nanostructures, *Analytical Chemistry* **87**, 230 (2015).
- [6] X. J. Zhou, Magnetism in medicine: A handbook, second completely revised and enlarged edition, *Medical Physics* **34**, 4978 (2007).
- [7] Q. H. Wang, A. Bedoya-Pinto, M. Blei, A. H. Dismukes, A. Hamo, S. Jenkins, M. Koperski, Y. Liu, Q.-C. Sun, E. J. Telford, H. H. Kim, M. Augustin, U. Vool, J.-X. Yin, L. H. Li, A. Falin, C. R. Dean, F. Casanova, R. F. L. Evans, M. Chshiev, A. Mishchenko, C. Petrovic, R. He, L. Zhao, A. W. Tsen, B. D. Gerardot, M. Brotons-Gisbert, Z. Guguchia, X. Roy, S. Tongay, Z. Wang, M. Z. Hasan, J. Wrachtrup, A. Yacoby, A. Fert, S. Parkin, K. S. Novoselov, P. Dai, L. Balicas, and E. J. G. Santos, The magnetic genome of two-dimensional van der Waals materials, *ACS Nano* **16**, 6960 (2022).
- [8] B. Huang, G. Clark, E. Navarro-Moratalla, *et al.*, Layer-dependent ferromagnetism in a van der Waals crystal down to the monolayer limit, *Nature* **546**, 270 (2017).
- [9] S. Jiang, L. Li, Z. Wang, K. F. Mak, and J. Shan, Controlling magnetism in 2D CrI_3 by electrostatic doping, *Nat. Nanotechnol.* **13**, 549 (2018).
- [10] N. Sethulakshmi, A. Mishra, P. Ajayan, Y. Kawazoe, A. K. Roy, A. K. Singh, and C. S. Tiwary, Magnetism in two-dimensional materials beyond graphene, *Materials Today* **27**, 107 (2019).
- [11] H. Vincent, D. Leroux, and D. Bijaoui, Crystal structure of $\text{Mn}_3\text{Si}_2\text{Te}_6$, *Journal of Solid State Chemistry* **63**, 349 (1986).
- [12] Y. Liu and C. Petrovic, Critical behavior and magnetocaloric effect in $\text{Mn}_3\text{Si}_2\text{Te}_6$, *Phys. Rev. B* **98**, 064423 (2018).
- [13] R. Rimet, C. Schlenker, and H. Vincent, A new semiconducting ferrimagnet: A silicon manganese telluride, *Journal of Magnetism and Magnetic Materials* **25**, 7 (1981).
- [14] L. M. Martinez, H. Iturriaga, R. Olmos, L. Shao, Y. Liu, T. T. Mai, C. Petrovic, A. R. Hight Walker, and S. R. Singamaneni, Enhanced magnetization in proton irradiated $\text{Mn}_3\text{Si}_2\text{Te}_6$ van der Waals crystals, *Applied Physics Letters* **116**, 172404 (2020).
- [15] A. F. May, Y. Liu, S. Calder, D. S. Parker, T. Pandey, E. Cakmak, H. Cao, J. Yan, and M. A. McGuire, Magnetic order and interactions in ferrimagnetic $\text{Mn}_3\text{Si}_2\text{Te}_6$, *Phys. Rev. B* **95**, 174440 (2017).
- [16] G. Kresse and J. Hafner, Ab initio molecular dynamics for liquid metals, *Phys. Rev. B* **47**, 558 (1993).
- [17] G. Kresse and J. Furthmüller, Efficiency of ab-initio total energy calculations for metals and semiconductors using a plane-wave basis set, *Computational Materials Science* **6**, 15 (1996).
- [18] G. Kresse and J. Furthmüller, Efficient iterative schemes for ab initio total-energy calculations using a plane-wave basis set, *Phys. Rev. B* **54**, 11169 (1996).

- [19] G. Kresse and D. Joubert, From ultrasoft pseudopotentials to the projector augmented-wave method, *Phys. Rev. B* **59**, 1758 (1999).
- [20] J. P. Perdew, K. Burke, and M. Ernzerhof, Generalized gradient approximation made simple, *Phys. Rev. Lett.* **77**, 3865 (1996).
- [21] P. E. Blöchl, Projector augmented-wave method, *Phys. Rev. B* **50**, 17953 (1994).
- [22] G. Kresse and D. Joubert, From ultrasoft pseudopotentials to the projector augmented-wave method, *Phys. Rev. B* **59**, 1758 (1999).
- [23] S. Grimme, Semiempirical gga-type density functional constructed with a long-range dispersion correction, *Journal of Computational Chemistry* **27**, 1787 (2006).
- [24] A. Togo and I. Tanaka, First principles phonon calculations in materials science, *Scr. Mater.* **108**, 1 (2015).
- [25] F. Jin, N. Lazarević, C. Liu, J. Ji, Y. Wang, S. He, H. Lei, C. Petrovic, R. Yu, Z. V. Popović, and Q. Zhang, Phonon anomalies and magnetic excitations in $\text{BaFe}_2\text{Se}_2\text{O}$, *Phys. Rev. B* **99**, 144419 (2019).
- [26] M. Moskovits and D. Dilella, Surface-enhanced Raman spectroscopy of benzene and benzene-d6 adsorbed on silver, *J. Chem. Phys.* **73**, 6068 (1980).
- [27] A. Dubroka, J. Humlíček, M. V. Abrashev, Z. V. Popović, F. Sapiña, and A. Cantarero, Raman and infrared studies of $\text{La}_{1-y}\text{Sr}_y\text{Mn}_{1-x}\text{M}_x\text{O}_3$ ($M = \text{Cr, Co, Cu, Zn, Sc}$ or Ga): Oxygen disorder and local vibrational modes, *Phys. Rev. B* **73**, 224401 (2006).
- [28] A. G. Souza Filho, J. L. B. Faria, I. Guedes, J. M. Sasaki, P. T. C. Freire, V. N. Freire, J. Mendes Filho, M. M. Xavier, F. A. O. Cabral, J. H. de Araújo, and J. A. P. da Costa, Evidence of magnetic polaronic states in $\text{La}_{0.70}\text{Sr}_{0.30}\text{Mn}_{1-x}\text{Fe}_x\text{O}_3$ manganites, *Phys. Rev. B* **67**, 052405 (2003).
- [29] A. Baum, A. Milosavljević, N. Lazarević, M. M. Radonjić, B. Nikolić, M. Mitschek, Z. I. Maranloo, M. Šćepanović, M. Grujić-Brojčin, N. Stojilović, M. Opel, A. Wang, C. Petrovic, Z. V. Popović, and R. Hackl, Phonon anomalies in FeS , *Phys. Rev. B* **97**, 054306 (2018).
- [30] N. Lazarević, M. Radonjić, M. Šćepanović, H. Lei, D. Tanasković, C. Petrovic, and Z. V. Popović, Lattice dynamics of KNi_2Se_2 , *Physical Review B* **87**, 10.1103/physrevb.87.144305 (2013).
- [31] U. Fano, Effects of configuration interaction on intensities and phase shifts, *Phys. Rev.* **124**, 1866 (1961).
- [32] S. Djurdjić Mijin, A. M. M. Abeykoon, A. Šolajić, A. Milosavljević, J. Pešić, Y. Liu, C. Petrovic, Z. V. Popović, and N. Lazarević, Short-range order in VI_3 , *Inorganic Chemistry* **59**, 16265 (2020).
- [33] L. J. Sandilands, Y. Tian, K. W. Plumb, Y.-J. Kim, and K. S. Burch, Scattering continuum and possible fractionalized excitations in $\alpha\text{-RuCl}_3$, *Physical Review Letters* **114**, 147201 (2015).
- [34] A. Milosavljević, A. Šolajić, J. Pešić, Y. Liu, C. Petrovic, N. Lazarević, and Z. V. Popović, Evidence of spin-phonon coupling in CrSiTe_3 , *Phys. Rev. B* **98**, 104306 (2018).
- [35] Y. Liu, Z. Hu, M. Abeykoon, E. Stavitski, K. Attenkofer, E. D. Bauer, and C. Petrovic, Polaronic transport and thermoelectricity in $\text{Mn}_3\text{Si}_2\text{Te}_6$ single crystals, *Phys. Rev. B* **103**, 245122 (2021).
- [36] Y. Ni, H. Zhao, Y. Zhang, B. Hu, I. Kimchi, and G. Cao, Colossal magnetoresistance via avoiding fully polarized magnetization in the ferrimagnetic insulator $\text{Mn}_3\text{Si}_2\text{Te}_6$, *Physical Review B* **103**, 161105 (2021).